PbI$_4$Cu$_2$(PPh$_3$)$_4$: A heterometallic iodide with unusual *cis*-divacant octahedral coordination sphere for lead: Synthesis, structure, red-infrared fluorescence and theoretical studies

Le-Qing Fan[a,b], Yi-Zhi Huang[a,b], Li-Ming Wu[a,*], Ling Chen[a,*], Jun-Qian Li[c], En Ma[a]

[a]*State Key Laboratory of Structural Chemistry, Fujian Institute of Research on the Structure of Matter, Chinese Academy of Sciences, Fuzhou, Fujian 350002, PR China*
[b]*Graduate School of the Chinese Academy of Sciences, Beijing 100039, PR China*
[c]*Department of Chemistry, Fuzhou University, Fuzhou, Fujian 350002, PR China*

Abstract

A new heterometallic iodide, PbI$_4$Cu$_2$(PPh$_3$)$_4$, was synthesized by reactions of PbI$_2$, CuI and triphenylphosphine (PPh$_3$) in DMF solution. The single-crystal X-ray diffraction analyses show that Pb(II) center adopts an unusual *cis*-divacant octahedral geometry. Crystal data: triclinic, space group $P\bar{1}$, $a = 12.3455(2)$ Å, $b = 13.8673(1)$ Å, $c = 21.3421(1)$ Å, $\alpha = 106.623(4)°$, $\beta = 103.478(6)°$, $\gamma = 93.574(5)°$, $V = 3371.83(6)$ Å^3 and $Z = 2$. Density function theory (DFT) calculations and fragment orbital interaction analyses reveal the presence of a three-center four-electron (3c–4e) hypervalent bonding about lead; and the formation of the unusual *cis*-divacant [PbI$_4$]$^{2-}$ octahedron is energetically favorable. The title yellow compound has an optical bandgap of 2.69 eV and shows remarkable red-infrared fluorescence emission at 732 nm with lifetime of 24 μs which is assigned as an iodine 5*p*-lead 6*s* to PPh$_3$-lead 6*p* charge transfer (XM-LM-CT).
© 2006 Elsevier Inc. All rights reserved.

Keywords: Heterometallic iodide; Crystal structure; *Cis*-divacant octahedral coordination; Red-infrared fluorescence

1. Introduction

A long-lasting interest in the photochemical and photophysical properties of d^{10} systems (especially of Cu$^+$ family) has been manifest for years [1]. There are more than 60 compounds with general formula Cu$_4X_4$L$_4$ where $X = $ alkynyl, halogen or alkoxy ligand, and L is an electron-pair donor such as a substituted pyridine or substituted phosphine. The structure motif of such polynuclear complexes is a "cubane" Cu$_4X_4$ core with copper and X atoms alternating at the corners, and additional L that completes the copper tetrahedral coordination sphere. Most interestingly, this type of compounds has been long known for their luminescence properties [2]. For example,

Cu$_4$I$_4$Py$_4$ (Py = pyridine) [3] presents remarkable fluorescence emissions at 619 and 438 nm with lifetimes of 25.5 and 23.2 μs, respectively, at 77 K. The high-energy emission that has been assigned to be an iodine-to-pyridine charge transfer (XLCT), as it seems to not be influenced by the structure of the Cu–I cubic backbone; whereas the low-energy emission depends on the Cu$_4$I$_4$ core and is not much influenced by the nature of ligand. Thus, a worthwhile question is to ask whether a heterometal ion could be introduced into the Cu–I skeleton that might change the electronic configurations, and therefore alter the luminescence property of the parent Cu–I complex.

In this paper, we present a new heterometallic iodide, PbI$_4$Cu$_2$(PPh$_3$)$_4$ (**1**), with a *cis*-divacant octahedral geometry for Pb(II) and show that the hetero lead atom does complicate the electronic structure and significantly change the photoluminescence property of the parent Cu–I compound. Density function theory (DFT) calculations

---

*Corresponding authors. Fax: +86 591 83704947.
E-mail addresses:* Liming_Wu@fjirsm.ac.cn (L.-M. Wu), chenl@fjirsm.ac.cn (L. Chen).

[4] and fragment orbital interaction analyses [5] reveal the presence of hypervalent bonding about lead and how this contributes to the formation of the unusual *cis*-divacant octahedron as a PbI_4Cu_2 group. The intense red-infrared fluorescence emission of **1** is assigned.

2. Experimental section

2.1. Materials and methods

All of the reagent-grade reactants were commercially available and employed without further purification. X-ray powder diffraction data were measured on a DMAX2500 diffractometer. Element analyses were performed on a Vario EL III element analyzer. Diffuse reflectance spectra were measured at room temperature with a PerkinElmer Lambda35 UV-Vis spectrometer equipped with an inte-

grating sphere. Fluorescence spectra were obtained at 10 K with the aid of an Edinburgh FLS920 fluorescence spectrophotometer with the polycrystalline sample held between two pieces of fused silica slices and cooled in a helium cryostat.

2.2. Synthesis of $PbI_4Cu_2(PPh_3)_4$ (**1**)

A mixture of PbI_2 (0.1 mmol, 0.046 g), CuI (0.2 mmol, 0.038 g) and PPh_3 (0.4 mmol, 0.105 g) was stirred in DMF (5 mL) for 10 min in air to ensure the solubility of each component and about 20 mL of i-PrOH was then diffused into the mixture. A 0.042 g yield of yellow crystals was obtained about 1 week (22.2% based on PbI_2). Anal. Calcd for **1** (dried) (%): C, 45.72; H, 3.20; N, 0. Found: C, 46.03; H, 3.45; N, ≤0.3.

2.3. Determination of crystal structure

Single-crystal X-ray diffraction measurements were performed on a Rigaku Mercury CCD diffractometer at room temperature with the aid of Mo$K\alpha$ radiation ($\lambda = 0.71073$ Å). The absorption was corrected by Crystal-Clear program, and the structure was solved by direct methods and refined with the aid of SHELXL-97 software package. All hydrogen atoms were calculated and refined using a riding model. The anisotropic refinement converged to $R_1 = 0.0301$, w$R_2 = 0.0644$ for $I > 2\sigma(I)$ data. Some refinement details and crystal data are gathered in Table 1. Selected bond lengths and angles are listed in Table 2. Crystallographic data have been deposited with the Cambridge Crystallographic Data Center as supplementary publication no. CCDC276304. Copies of the data can be obtained free of charge on application to CCDC, 12 Union Road, Cambridge CB2 1EZ, UK (fax: +44 1223 336 033; E-mail: deposit@ccdc.cam.ac.uk).

Table 1
Crystallographic data and refinement details for compound **1**

Formula	$PbI_4Cu_2P_4C_{72}H_{60}$
Fw	1890.98
Cryst system	Triclinic
Space group, Z	$P\bar{1}$, 2
a (Å)	12.3455(2)
b (Å)	13.8673(1)
c (Å)	21.3421(1)
α (deg)	106.623(4)
β (deg)	103.478(6)
γ (deg)	93.574(5)
V (Å^3)	3371.83(6)
D_c (g · cm^{-3})	1.863
μ (mm^{-1})	5.082
GOF on F^2	1.035
R_1, wR_2 ($I > 2\sigma(I)$)[a]	0.0301, 0.0644
R_1, wR_2 (all data)	0.0377, 0.0684

[a] $R_1 = \Sigma||F_o| - |F_c||/\Sigma|F_o|$, w$R_2 = [\Sigma w(F_o^2 - F_c^2)^2/\Sigma w(F_o^2)^2]^{1/2}$.

Table 2
Selected bond lengths (Å) and angles (deg) for compound **1**

	Exp.	Calcd.		Exp.	Calcd.
Pb–I(1)	3.0172(3)	3.06	I(3)–Cu(2)	2.7345(5)	2.88
Pb–I(2)	3.1573(3)	3.23	I(4)–Cu(2)	2.6871(5)	2.78
Pb–I(3)	2.9895(3)	3.04	Cu(1)–P(1)	2.267(1)	2.38
Pb–I(4)	3.2186(3)	3.27	Cu(1)–P(2)	2.277(1)	2.40
I(1)–Cu(1)	2.7796(5)	2.87	Cu(2)–P(3)	2.254(1)	2.39
I(2)–Cu(1)	2.7210(5)	2.80	Cu(2)–P(4)	2.265(1)	2.40
I(1)–Pb–I(2)	90.839(9)	91.10	P(2)–Cu(1)–I(1)	100.46(3)	104.39
I(1)–Pb–I(4)	100.333(9)	98.96	P(2)–Cu(1)–I(2)	100.65(3)	103.77
I(2)–Pb–I(4)	167.596(8)	165.34	I(2)–Cu(1)–I(1)	106.20(2)	104.97
I(3)–Pb–I(1)	92.220(8)	96.53	P(3)–Cu(2)–P(4)	125.18(4)	125.89
I(3)–Pb–I(2)	97.632(9)	99.32	P(3)–Cu(2)–I(3)	104.03(3)	104.66
I(3)–Pb–I(4)	87.383(9)	90.14	P(3)–Cu(2)–I(4)	112.39(3)	111.67
P(1)–Cu(1)–P(2)	136.22(4)	129.02	P(4)–Cu(2)–I(3)	100.78(3)	101.24
P(1)–Cu(1)–I(1)	108.25(3)	107.81	P(4)–Cu(2)–I(4)	107.23(3)	106.27
P(1)–Cu(1)–I(2)	102.14(3)	104.72	I(4)–Cu(2)–I(3)	104.66(2)	104.75

2.4. Calculation method

DFT calculations [4] were performed at B3LYP level using GAUSSIAN-98 software package [6]. The LANL2DZ effective core potentials and basis sets were used to describe Pb, I, Cu and P [7], while the standard 6-31G basis set was for C and H. Polarization functions were also added for Pb, P and I, i.e. $Pb(\xi(d) = 0.164)$, $P(\xi(d) = 0.34)$ and $I (\xi(d) = 0.266)$ [8]. A relativistic core potential LANL RECP (the LANL2DZ basis set) are using for accounting the relativistic effects of heavier atoms [9].

3. Results and discussion

3.1. Structure description

The discrete molecular structure of **1** is shown in Fig. 1 and the view slightly off [100] of the triclinic structure is shown in SFig. 1, and important bond distances and bond angles are given in Table 2. The remarkable feature of the Pb coordination sphere, compare to the most frequently occurring octahedral geometry in lead halide chemistry, is the unusual incomplete octahedron (with two vacant equatorial sites). The axial (ax) I(2)–Pb–I(4) angle is $167.596(8)^\circ$, around a 12° deviation from the ideal octahedral symmetry, and the equatorial (eq) I(1)–Pb–I(3) angle is $92.220(8)^\circ$ which suggest that this geometry is not a classical trigonal bipyramid with a $6s^2$ lone pair finishing out the equatorial group. The geometry of the central Pb coordination sphere is comparable to that in mononuclear $[Bu_3N–(CH_2)_2–NBu_3][PbI_4]$ [10a], where $I_{(ax)}–Pb–I_{(ax)} = 153.56^\circ$, $I(eq)–Pb–I(eq) = 95.48^\circ$. The axial angular difference of these two is 14°, which comes from the increasing of the electronegativity of iodine atoms by the bonding interaction with copper ions. The concerned geometry data for some other related species are listed in Table 3. Those angular data show that the axial X–M–X angle is increased with the increasing of electronegativity of halogen, from I to Cl, and becomes closer to the ideal linear geometry. The equatorial Pb–I distances 2.9895(3) and 3.0172(3) Å are shorter than the axial ones 3.2186(3) and 3.1573(3) Å, but both are comparable to those in mononuclear $[Bu_3N–(CH_2)_2–NBu_3][PbI_4]$ [10a], where Pb–I(eq) = 2.9116(8), 3.005(1) Å, and Pb–I$_{(ax)}$ = 3.2803(8),

3.1457(9) Å, respectively; and the most frequently occurring iodoplumbates with octahedral PbI_6 unit, e.g. 3.175(2)–3.200(2) Å in the layered perovskites compound $(C_4H_9NH_3)_2PbI_4$ [11a], and 3.137(1)–3.264(5) Å in bilayered perovskite $Pb_2I_7^{3-}$ [11b]. The recent example of such *cis*-divacant octahedral geometry for a $6s^2$ ion is the $BiCl_2I_2^-$ anion [12], in which the Cl ions are found in the axial, and the I anions, in the equatorial positions, but the reason for its arrangement is unclear (see more in theoretical analyses section). The only trinuclear lead halide analog of **1** is a bent sandwich arene chloride $(C_6H_4Me_2)_2 [Pb(AlCl_4)_2]$ [13], where axial and equatorial Cl–Pb–Cl angles are 139.31° and 69.34°. Since the totally different property of the ligand $AlCl_4^-$ vs. $CuI_2(PPh_3)_2^-$, and the different bonding involvement of arene with the lead ion (ring-carbon distances are in the range 3.07–3.29 Å vs. those in **1** 3.28–4.94 Å), these two structures are remote related. Both Cu1 and Cu2 in **1** have the common four coordination by two μ_2-I^- ions and two P atoms from PPh_3 in a distorted tetrahedral symmetry with an average tetrahedral angle 109.02°. The Cu–I and Cu–P distances are 2.6871(5)–2.7796(5) Å and 2.254(1)–2.277(1) Å, respectively, which are comparable to those in typical cubane-like $Cu_4(\mu_3–I)_4(PPh_3)_4$ (2.653–2.732 Å, and 2.242–2.258 Å) [14]. The Pb···Cu(1) and Pb···Cu(2) distances are 3.73(2) and 3.76(2) Å, respectively, which indicate no significant Pb–Cu bonding interaction.

3.2. Theoretical analyses

The coordination of the Pb(II) in **1** by four iodine ligands is not as a tetrahedron with T_d symmetry (that should be favorite from a simple symmetry point of view), but a *cis*-divacant octahedron (close to C_{2v}), which structurally shows a close relationship to the most frequently occurring PbI_6 octahedral geometry. This unusual geometry encouraged us to perform a series of theoretical computations at the B3LYP level of DFT. Firstly, the geometry of discrete molecular **1** was fully optimized, giving the selected structure parameters listed in Table 2. The calculated bond lengths, angles, and dihedral angles differ from the experimental ones by 0.04–0.14 Å, $0.1–7.2^\circ$ and $0.3–4.0^\circ$, respectively. It indicates the rationality of our geometry optimization if the infinite packing in the real crystal is not considered. Further calculations were performed on a hypothetical isolated PbI_4^{2-} complex. The optimized minimum-energy-structure of PbI_4^{2-} complex without any limitation is a tetrahedron, which is of the highest symmetry for four coordinated species. However, the energy of equilibrium structure of PbI_4^{2-} with a C_{2v} symmetry constraint (*cis*-divacant octahedron), is higher than the minimum with T_d symmetry but only by 49.2 kJ mol^{-1}. Such small energy difference suggests that a structure of *cis*-divacant octahedral PbI_4^{2-} is possible. In addition, the C_{2v} structure involves a three-center four-electron (3c-4e) bonding that benefits the stabilization of the parent structure [15]. Hoffmann et al. [15] pointed out

Table 3
Selected bond angles (deg) for some cis-divacant octahedral ns^2 metal halides

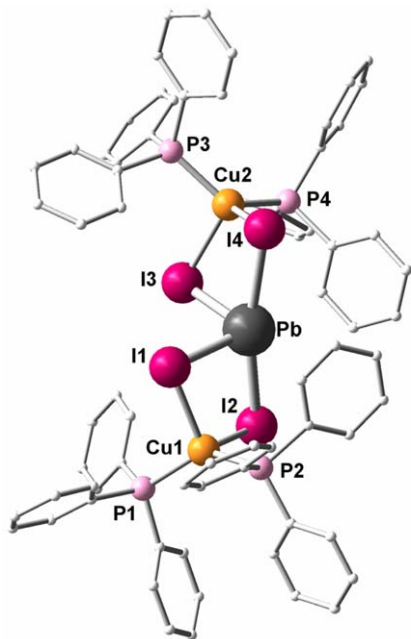| Compound	X–M–X angle		Refs.
	Axial	Equatorial	
1	167.60	92.22	This work
$[Bu_3N–(CH_2)_2–NBu_3][PbI_4]$	153.56	95.48	[10a]
$[BzL_4P]_2[PbBr_4]$	166.27	95.77	[10b]
$BiCl_2I_2^-$	170.51	95.61	[12]

Fig. 1. The molecular structure of the isolated $PbI_4Cu_2(PPh_3)_4$ complex in **1**. Hydrogen atoms are omitted for clarity.
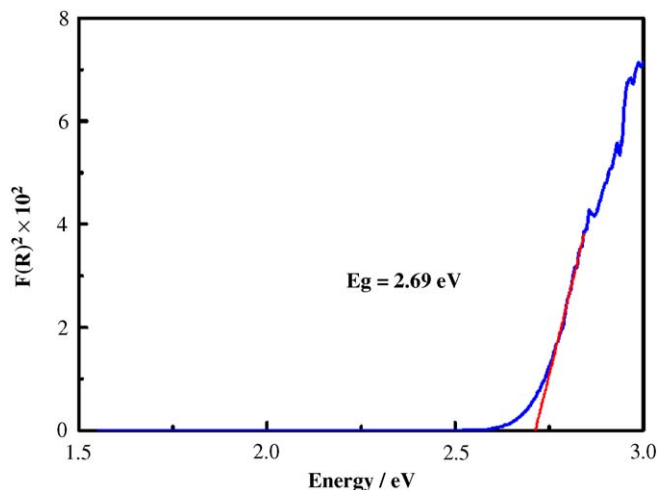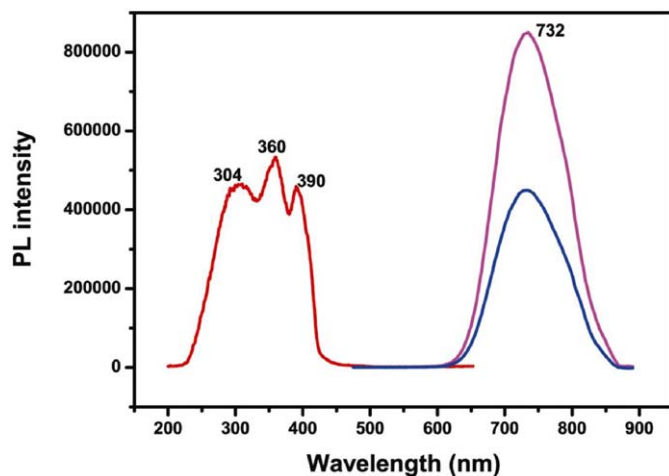

Fig. 2. Plot of $F(R)^2$ vs. photon energy for **1**.

Fig. 3. The solid-state emission and excitation spectra of polycrystalline **1** at 10 K. Emission spectrum (magenta), $\lambda_{max} = 732$ nm, excitation wavelength is at 358 nm, while blue one is excited at 390 nm, with maximum = 732 nm and $\tau = 25\,\mu s$; and excitation spectrum (red) is of emission at 732 nm.

that ligands with larger electronegativities favor an electron-rich hypervalent bonding on the basis of qualitative orbital analyses. Such a conclusion has also been confirmed in this specific case by our calculations, that is, the optimized minimum-energy-geometry for PbF_4^{2-} is a butterfly structure with C_{2v} symmetry, and for other PbX_4^{2-} (X = Cl, Br, I) are T_d symmetry structures. Compare to the available experimental results (Table 3), a distortion is obvious, but the trend is confirmed, that is from I to Cl, the axial X–M–X angle for MX_4 is getting closer to the linear configuration. Here, the axial angle in **1** is between those of $PbBr_4^{2-}$ and $BiCl_2I_2^{-}$, an increase of the electronegativity of the iodine atoms is considered to come from the strong interactions with each of the two copper ions. The coordinate bonding between I^- and Cu^+ weaken the ability of I^- to donate electron to Pb^{2+}, i.e., the coordination of iodine with copper atoms apparently results in the improvement of its electronegativity. As a result, a 3c-4e bonding close to linear is favorable (the axial I(2)–Pb–I(4) angle is 167.596(8)°). For the same reason, it is now easy to understand the arrangement of the $BiCl_2I_2^{-}$ anion [12], in which the more electronegative chlorine ions take the linear axial positions to favor the Cl–Bi–Cl hypervalent bonding.

3.3. Diffuse reflectance spectroscopy

The optical band gap of **1** was assessed to be 2.69 eV by studying its diffuse reflectance spectroscopy (Fig. 2). The optical band gap is consistent with the yellow color of **1**. According to the Kubelka–Munk function: $F(R) = (1 - R)^2/2R$, in which R is the experimentally observed

reflectance [16], the bandgap is determined as the intersection point of the energy axis with the extrapolated linear portion of the absorption edge in an $F(R)^2$ vs. photon energy plot.

3.4. Fluorescent analysis

The solid-state emission spectrum of **1** at 10 K is shown in Fig. 3. Excitation of the polycrystalline sample at $\lambda = 358$ nm produces an intense red-infrared emission with peak maximum at 732 nm ($\tau = 24\,\mu s$). This emission band can be assigned as an iodine $5p$-lead $6s$ to PPh_3-lead $6p$ charge transfer, i.e., halide and metal-to-ligand and metal charge transfer (XM-LM-CT). Details are discussed below.

As to one of the counterparts of **1** without Pb(II), $Cu_4I_4Py_4$, the analyses on its molecular orbitals (MOs) by
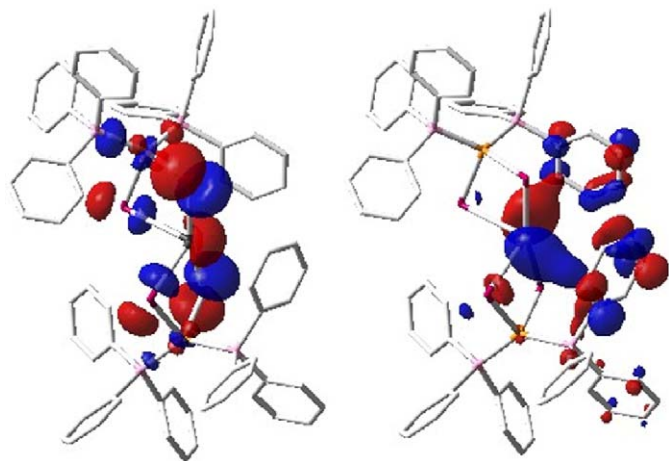
Fig. 4. The HOMO (left) and LUMO (right) of **1**.

Ford and co-workers have established that its emission at 438 nm comes from halide-to-ligand charge transfer (XLCT) exited states [3a]. Similarly, we checked the frontier MOs of **1** at the B3LYP level of DFT. It should be no surprise that the introduction of Pb(II) obviously complicates the orbital configurations of **1**. On one hand, the 11 highest energy MOs among the occupied ones of **1** are mainly iodine 5p (31–71%) in character, with marked mixing with the ligand orbitals (PPh$_3$) (8–40%) and copper 3d orbitals (6–28%) (STable 3). In contrast, a nonnegligible contribution of 16% lead 6s is observed in the highest occupied orbital (HOMO). The HOMO appears antibonding through out-of-phase mixing of lead 6s and iodine 5p (see Fig. 4, left). This antibonding pattern suggests an increase in the HOMO energy relative to Cu$_4$I$_4$(Py)$_4$, in which the main character of the HOMO is nonbonding iodine 5p [3a]. On the other hand, the 26 lowest unoccupied MOs are aromatic cycles π^* (51–94%) in essence, and five of them have more than 10% lead 6p components. Especially in the lowest unoccupied molecular orbital (LUMO), the two contributions are 55% and 26%, respectively. As shown in Fig. 4 (right), they are somewhat bonding through in-phase mixing, which suggests a decrease in energy from the pure ligands π^* orbitals of the LUMO. The molecular orbital correlation diagram of **1** is shown in SFig. 2. In summary, the HOMO–LUMO gap of **1** decreases by the inclusion of 6s and 6p orbitals of Pb(II). And thus, we can understand that **1** realizes fluorescent emissions when excited at a lower energy (390 nm) than the 365 nm at which Cu$_4$I$_4$Py$_4$ realizes XLCT [3a].

4. Conclusions

A new heterometallic Pb/Cu iodide, PbI$_4$Cu$_2$(PPh$_3$)$_4$ **1**, with unusual *cis*-divacant PbI$_4$ octahedral geometry has been successfully synthesized. Calculations show that such C_{2v} symmetry motif is energetically favorable, the stability also increasing because I–Pb–I hypervalent bonding favors

a linear configuration. The yellow compound **1** has an optical bandgap of 2.69 eV and shows remarkable red-infrared fluorescence emission which is assigned as an iodine 5p-lead 6s to PPh$_3$-lead 6p charge transfer (XM–LM–CT). The LUMO–HOMO gap of **1** is narrowed by introduction of lead component to Cu–I skeleton compared to that in the Cu$_4$I$_4$L$_4$ complex [3a]. If a cubane-like Cu$_x$M$_{4-x}$I$_4$L$_4$ can be made, the comparison of the role of the heterometal ion will be more direct.

Appendix A. Supplementary data

Crystallographic data have been deposited with the Cambridge Crystallographic Data Center as supplementary publication no. CCDC276304. Crystallographic informationfile (CIF), detailed tables of atomic coordinates, anisotropic thermal parameters, detailed bond lengths and angles, contributions to the molecular orbitals and the molecular orbital diagram. These materials are available free of charge via the Internet at doi:10.1016/j.jssc. 2006.04.019.

References

[1] (a) M. Vitale, P.C. Ford, Coord. Chem. Rev. 219–221 (2001) 3–16;
    (b) E. Cariati, D. Roberto, T. Ugo, P.C. Ford, S. Galli, A. Sironi, Inorg. Chem. 44 (2005) 4077–4085;
    (c) V.W.-W. Yam, C.H. Lam, N. Zhu, Inorg. Chim. Acta 331 (2002) 239–245.
[2] (a) F.G. Mann, D. Purdie, A.F. Wells, J. Chem. Soc. (1936) 1503–1513;
    (b) H.D. DeAhna, H.D. Hardt, Z. Anorg. Allg. Chem. 387 (1972) 61–71.
[3] (a) M. Vitale, W.E. Palke, P.C. Ford, J. Phys. Chem. 96 (1992) 8329–8336;
    (b) A. Vega, J.Y. Saillard, Inorg. Chem. 43 (2004) 4012–4018.
[4] (a) A.D. Becke, J. Chem. Phys. 98 (1993) 5648–5652;
    (b) B. Miehlich, A. Savin, H. Stoll, H. Preuss, Chem. Phys. Lett. 157 (1989) 200–206;
    (c) C. Lee, W. Yang, G. Parr, Phys. Rev. B 37 (1988) 785–789.
[5] T.A. Albright, J.K. Burdett, M.H. Whangbo, Orbital Interactions in Chemistry, Wiley, New York, 1985.
[6] M.J. Frisch, G.W. Trucks, H.B. Schlegel, G.E. Scuseria, M.A. Robb, J.R. Cheeseman, V.G. Zakrzewski, J.A. Montgomery Jr, R.E. Stratmann, J.C. Burant, S. Dapprich, J.M. Millam, A.D. Daniels, K.N. Kudin, M.C. Strain, O. Farkas, J. Tomasi, V. Barone, M. Cossi, R. Cammi, B. Mennucci, C. Pomelli, C. Adamo, S. Clifford, J. Ochterski, G.A. Petersson, P.Y. Ayala, Q. Cui, K. Morokuma, D.K. Malick, A.D. Rabuck, K. Raghavachari, J.B. Foresman, J. Cioslowski, J.V. Ortiz, B.B. Stefanov, G. Liu, A. Liashenko, P. Piskorz, I. Komaromi, R. Gomperts, R.L. Martin, D.J. Fox, T. Keith, M.A. Al-Laham, C.Y. Peng, A. Nanayakkara, C. Gonzalez, M. Challacombe, P.M.W. Gill, B. Johnson, W. Chen, M.W. Wong, J.L. Andres, C. Gonzalez, M. Head-Gordon,

E.S. Replogle, J.A. Pople, Gaussian 98 (Revision A.7), Gaussian, Inc., Pittsburgh, PA, 1998.

[7] (a) P.J. Hay, W.R. Wadt, J. Chem. Phys. 82 (1985) 270–310;
     (b) W.R. Wadt, P.J. Hay, J. Chem. Phys. 82 (1985) 284–298.

[8] S. Huzinaga, J. Andzelm, M. Klobukowski, E. Radzio-Andzelm, Y. Sakai, H. Tatewaki, Gaussian Basis Sets for Molecular Calculations, Elsevier, Amsterdam, 1984.

[9] C. Check, T. Faust, J. Bailey, B. Wright, T. Gilbert, L. Sunderlin, J. Phys. Chem. A 105 (2001) 8111–8116.

[10] (a) H. Krautscheid, F. Vielsack, Z. Anorg. Allg. Chem. 625 (1999) 562–566;
     (b) H. Groger, C. Lode, H. Vollmer, H. Krautscheid, Z. Anorg. Allg. Chem. 628 (2002) 57–62.

[11] (a) D.B. Mitzi, Chem. Mater. 8 (1996) 791–800;
     (b) X.-H. Zhu, N. Mercier, A. Riou, P. Blanchard, P. Frère, Chem. Commun. (2002) 2160–2161.

[12] A.M. Goforth, M.D. Smith, L. Peterson, H. Loye, Inorg. Chem. 43 (2004) 7042–7049.

[13] W. Frank, F. Wittmer, Chem. Ber. 130 (1997) 1731–1732.

[14] J.C. Dyason, P.C. Healy, L.M. Engelhardt, C. Pakawatchai, V.A. Patrick, C.L. Raston, A.H. White, J. Chem. Soc. Dalton Trans. (1985) 831–838.

[15] G.A. Landrum, N. Goldberg, R. Hoffmann, J. Chem. Soc. Dalton Trans. (1997) 3605–3613.

[16] G. Cao, L.K. Rabenberg, C.M. Nunn, T.E. Mallouk, Chem. Mater. 3 (1991) 149–156.